Journal of Thermal Analysis and Calorimetry (2025) 150:4279–4294
https://doi.org/10.1007/s10973-025-14006-0

Performance improvement of high-density data center via two-phase liquid immersion cooling

Nada M. Mohammed[1] · Wael M. El-Maghlany[1] · Mohamed Elhelw[1] · Ahmed H. Abdelaziz[1]

Received: 5 May 2024 / Accepted: 16 January 2025 / Published online: 22 February 2025
© The Author(s) 2025

Abstract

This paper introduces two distinct approaches for efficiently cooling high-density data centers with a capacity of up to 1168 kW, aiming to achieve the optimal cooling method for extracting heat from electronic servers. The investigation involves a comparative analysis between air-based cooling, incorporating modifications to hot aisle containment, and liquid-based cooling utilizing a two-phase immersion system. Three-dimensional simulations are conducted employing computational fluid dynamics (CFD) analysis. Furthermore, the simulation examines the influence of introducing copper coating materials to server components in liquid cooling, varying the thickness to enhance heat transfer efficiency. The analysis demonstrates that, in liquid cooling, the maximum server temperature diminishes to 65 °C, and power usage effectiveness improves from 2 in the air cooling system to 1.01 in liquid cooling. The application of copper coating results in a 13% enhancement in the gradual temperature distribution among servers, especially in high-power servers, and eliminates most hot spots by decreasing the maximum temperature. However, the simulation indicates a comparatively modest temperature improvement of 8% when coating low-power servers.

Keywords Data center · Immersion cooling · Copper coating · Power effectiveness

List of symbols

E	Energy (J)
J`	Net mass flux over the vapor–liquid interface ($kg.m^{-2}\ S^{-1}$)
k	Turbulent kinetic energy ($m^2.S^{-2}$)
M	Molecular weight ($kg.kmol^{-1}$)
p	Pressure (Pa)
R	Gas constant ($J.mol^{-1}.\ K^{-1}$)
S	Source term in conservation equation
T	Temperature (K)
t	Time (S)
u	Velocity in X-direction ($m.s^{-1}$)
ν	Velocity in Y-direction ($m.s^{-1}$)
w	Velocity in Z-direction ($m.s^{-1}$)

Greek Symbols

ρ	Density ($kg.m^{-3}$)
α	Accommodation
μ	Eddy viscosity (Pa.S)
τ	Shear-rate tensor
ε	Turbulent dissipation rate
λ	Temperature distribution percentage

Subscripts

c	Coefficient
l	Liquid
M	Momentum
t	Turbulent
v	Vapor
sat	Saturation

Abbreviations

ASHRAE	American society of heating, refrigerating and air-conditioning engineers
CRAC	Computer room air-conditioning
CRAH	Computer room air handling
CFD	Computational fluid dynamics
FC	Fluorocarbon
HAC	Hot aisle containment
IT	Information technology
PUE	Power usage effectiveness
RA	Return air

✉ Wael M. El-Maghlany
elmaghlany@alexu.edu.eg; elmaghlany@yahoo.com

[1] Mechanical Engineering Department, Faculty of Engineering, Alexandria University, Alexandria, Egypt

Introduction

Data centers are server rooms in any business organization, institution, or government agency.

They provide capabilities of centralized storage, backups, and networking of data. Data centers include IT racks that contain servers, storage devices, and network cabling. The power consumption of servers results in heat generation, necessitating the implementation of air-conditioning systems to ensure optimal functioning and prevent potential shutdowns. Elevated temperatures pose a risk of equipment malfunction or damage, with internal components susceptible to burning up. The rate of temperature increase directly impacts the failure rate of electronic circuits. Because data centers operate 24 h a day and 365 days a year, the cooling system must be designed to achieve continuous heat extraction to avoid failure [1]. The widespread adoption of internet applications has led to the rapid growth of high-density data centers in recent years, resulting in significant energy consumption challenges. Projections indicate that large-scale data centers are anticipated to account for around 20% of the world's total energy consumption by the year 2030 [2]. The primary contributors to the high energy consumption in data centers are the IT equipment, cooling system, power distribution, and other associated requirements. Specifically, the cooling system alone can constitute as much as 40% of the average energy consumption [3], so cooling procedures have a significant interest in achieving efficient energy and saving costs. Also, CO_2 emissions due to electric consumption represent a massive problem to the world [4]. Most researchers consider that the maximum allowable temperature for servers to avoid malfunctions is 85 °C; however, for storage devices, the server's temperature should not exceed 45 °C [5]. The prevalent method for cooling servers is through an air-cooled system, commonly employing CRAC units that are connected to the room. The function of these units is to cool the room, utilizing either a hard floor or raised floor setup. Cold air is released by the CRAC units beneath the raised floor, and perforated tile vents in the cold aisles of the raised floor distribute this cold air to the front of racks that are positioned facing each other. Subsequently, the hot air exits through the back of the racks into the hot aisles, facilitating the return of air to the CRAC units [6, 7]. ASHRAE recommends operating conditions for cooling air with a dry bulb temperature ranging from 18 °C to 27 °C. Additionally, it is advised to maintain humidity within specific parameters, including a dew point temperature of 5.5 °C, relative humidity at 60%, and a dew point temperature of 15 °C [8, 9].

The air-cooled system encounters several challenges, including a low heat transfer coefficient and increased

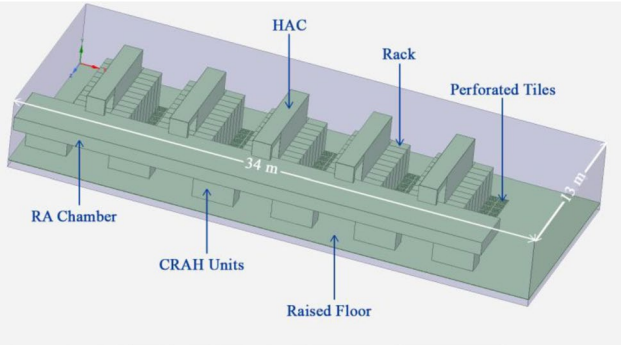


Fig. 1 Air-cooled system

Table 1 Rack types

Racks	A-type	B-type
Number	40	60
Number of servers per rack	48	42
Rack area/m^2	0.6 × 1.2	0.6 × 1.2
Height /m	2.4	2
Power per rack /kW	16	8.8

complexity [4]. An alternative cooling method is liquid cooling, where a liquid acts as a coolant, flowing across the hot server components to dissipate heat. This is achieved by utilizing a dielectric fluid that does not conduct electricity. Liquids possess a significantly higher heat capture capacity per unit volume compared to air. This approach enables the liquid to extract heat more effectively, resulting in a higher liquid supply temperature compared to air cooling. The dissipated heat is then released into the atmosphere, and in some cases, it may be reused through a heat exchanger [10]. Implementing hot or cold aisle containment stands out as one of the most effective strategies for enhancing energy efficiency in a data center, as it enables the separation of air streams, mitigating issues related to air recirculation and bypass [11]. Ni et al. [12] demonstrated that HAC represents the optimal solution for improving cooling performance. Two distinct air distribution methods, namely, row-based and rack-based cooling solutions, are employed to enhance cooling efficiency. Both in-row and rack-based cooling systems offer the advantage of shorter airflow paths, reducing fan power and eliminating recirculation [13]. Rack-based cooling can support power density up to 50 kW per rack. However, rack-based and in-row cooling needs higher capital costs than room cooling due to a higher number of cooling units. Moazamigoodarzi et al. [14] demonstrated that the in-row cooling approach enhances air flow distribution and improves overall cooling performance. Jin et al. [15] conducted a comparative analysis of energy efficiency

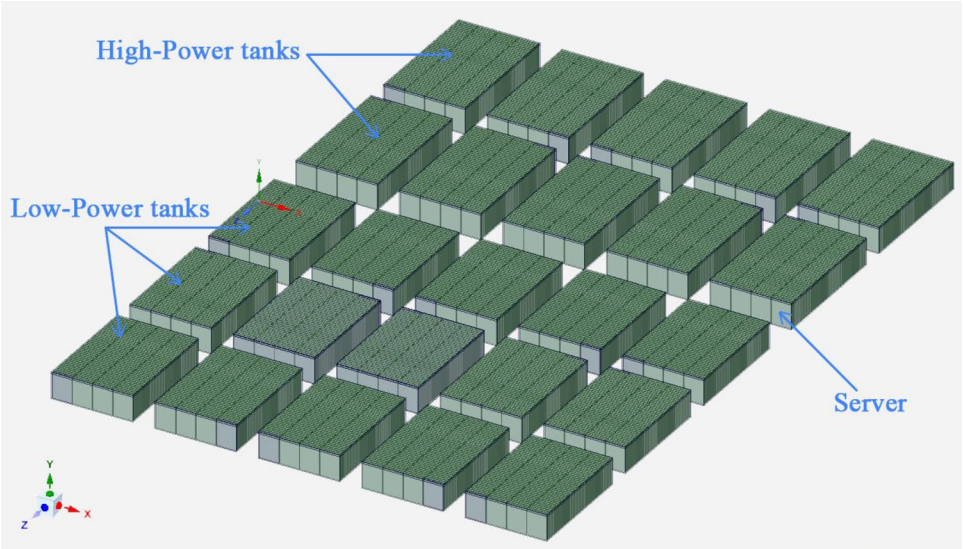


Fig. 2 Liquid-cooled system

Table 2 Details of server tanks

Tank	High-power	Low-power
Dimensions /m^3	1.875×2.985×0.615	1.875×2.617×0.615
Number of servers per tank	192	168
Server dimensions /m^3	0.45×0.6×0.0445	0.45×0.6×0.0445
Total power per tank /kW	64	35.2

between room cooling with raised floor and in-row-based systems for cooling data centers, revealing that in-row-based cooling exhibits superior thermal performance and higher energy efficiency when compared to raised floor room cooling.

Liquid cooling can dissipate heat higher than conventional air cooling [2] attributed to its higher heat transfer coefficient [15]. Various liquid cooling approaches exist, including single-phase direct-to-chip liquid cooling, single-phase immersion cooling, two-phase direct-to-chip liquid cooling, and two-phase immersion cooling. In the case of two-phase immersion cooling, IT components are completely submerged in dielectric liquid. Heat is extracted from servers through the evaporation of the dielectric liquid coolant, which has a low boiling point. The vapor is subsequently condensed through heat exchanger coils, completing the cycle [16]. This method not only reduces power consumption and noise by eliminating air conditioners and fans present in air-cooled systems but also lowers PUE. PUE is the ratio between the total data center energy and the IT equipment energy [17], where the total data center energy includes the energy consumed by IT equipment as well as the energy required for cooling. When cooling energy is reduced, the PUE approaches to 1, indicating a more efficient system. Zhang et al. [18] conducted

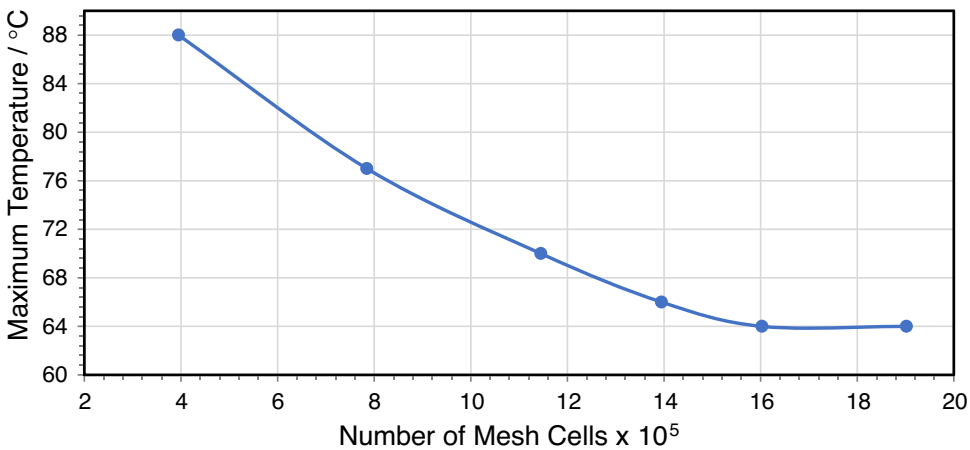


Fig. 3 Mesh dependence for high-power tank

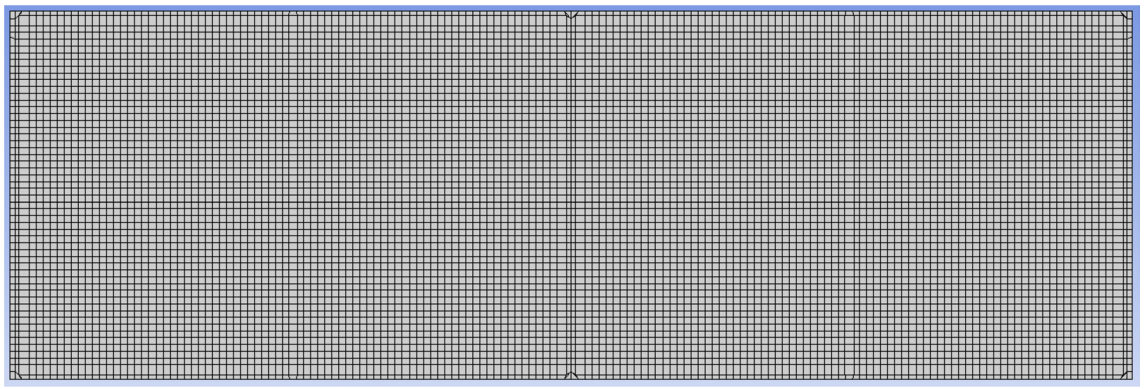


Fig. 4 Mesh at front servers' plane, *X*–*Y* view

Table 3 FC-72 Oil Properties [28]

Properties	Liquid/phase1	Vapor/phase2
Density /kg.m^{-3}	1680	13.1
Viscosity /Pa.S	0.00064	0.000124
Specific heat /J.kg^{-1}.°C^{-1}	1100	900
Thermal conductivity/ W.m^{-1}.°C^{-1}	0.057	0.0235
Average molecular weight	338	338

simulations on an integrated indirect liquid cooling system designed for edge data centers, comparing its performance with air cooling. Kuncoro et al. [19] proposed a cooling model aimed at enhancing the energy efficiency of data centers through the utilization of various fluid types. Liu and Yu [20] conducted a comparative analysis between laboratory experiments and CFD simulations to assess the performance of a two-phase liquid cooling system. This study also investigated the intervals between submerged servers at different loads and their impact on surface temperatures. An et al. [21] presented a three-dimensional simulation of a two-phase immersion cooling solution for high-density powered processor designs using ANSYS Fluent. Watson and Venkiteswaran [22] investigated two different types of cooling systems: an air cooling system with HAC and a single-phase liquid immersion cooling. Eiland et al. [23] conducted a study involving a single server fully immersed horizontally in mineral oil, demonstrating that the use of mineral oil significantly reduced the system's thermal resistance compared to traditional air room cooling. Luo et al. [24] investigated the influence of the SiC/white mineral oil-based nanofluids as a new coolant on immersion cooling. Ali [25] simulated the thermal and stress analysis of enhanced copper spreaders for electronic chip nucleate boiling immersion cooling.

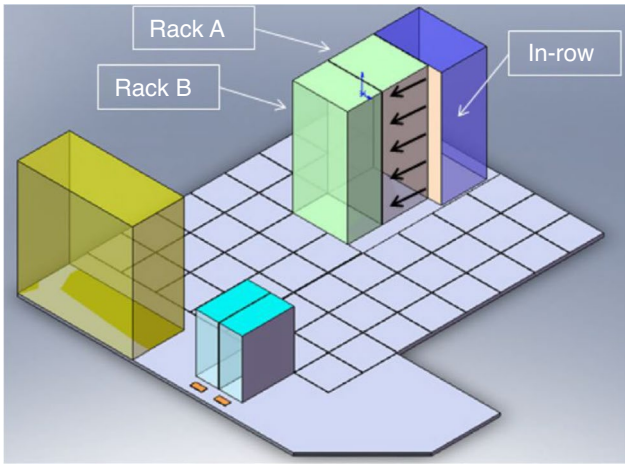


Fig. 5 Data center layout

Scope, objective and methodology

The elevation in server temperature significantly impacts server performance, posing a considerable challenge, especially given the growing dependence on data centers to manage systems in our daily lives. Previous research has predominantly focused on examining a limited number of electronic chips and servers, with insufficient exploration into the effects of oil cooling on the thermal and power efficiency of integrated high-density data centers. The present study aims to eliminate the huge power consumption and cost associated with data center cooling systems, while also contributing to environmental conservation by reducing CO_2 emissions. The research involves a comparative analysis, employing three-dimensional full-scale modeling, between a two-phase immersion liquid cooling system and an air-cooled system through ANSYS 18.1, CFD analysis. In the liquid-cooled system, servers are fully immersed in tanks containing dielectric oil with a low boiling point to enhance

cooling efficiency. In the air-cooled system, server racks are mounted on a raised floor, and HAC is implemented to prevent hot air recirculation. Additionally, the study explores the impact of adding a copper coating to servers to improve liquid cooling efficiency. The analysis includes temperature distribution among servers and PUE for all scenarios.

Proposal systems

The evaluation of cooling methodologies is conducted within high-density data center. For conventional geometry of the server air-cooled system [26], a three-dimensional IT server room is simulated with dimensions measuring 34×13 m^2 and a height of 4.8 m. The raised floor is configured at a height of 0.5 m, featuring 10 rows, each containing 10 racks. Spacings for hot and cold aisles are set at 1.2 and 1.8 m, respectively. The raised floor comprises perforated tiles measuring 0.6×0.6 m^2, with a porosity of 25%, while the racks have a porosity of 35%. Six CRAH units are employed to cool the servers, with an inlet air temperature set at 16 °C. HAC is installed and connected to the RA chamber, as illustrated in Fig. 1. HAC is considered as an enclosure for the hot air exits from servers and sends this hot air to the return air (RA) chamber then to CRAH units for continuous cooling. The IT server room accommodates two types of racks, namely, A-Type (high-power) and B-Type (low-power), with total power of 1168 kW, as indicated in Table 1.

In the liquid-cooled system, the configuration involves two types of tanks: 10 tanks designated for high-power racks and 15 tanks allocated for low-power racks, as shown in Fig. 2. Each tank accommodates four racks, and servers are vertically immersed in the tanks filled with dielectric oil FC-72, serving as the coolant. The servers are spaced apart with a gap of 15 mm between them. The specifics for the two types of tanks in the liquid-cooled setup are detailed in Table 2.

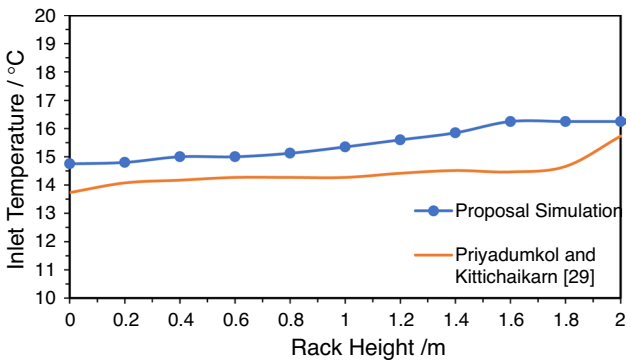


Fig. 6 Inlet temperature in rack A

Various mesh element cells are simulated to achieve solution convergence and obtain accurate results with improved mesh quality and reduced computational time, as illustrated in Fig. 3. The assembly mesh method utilized is the cut cell approach with an average element quality of 0.94. The total number of mesh cells for high-power and low-power tanks are 1,603,584 and 1,272,544 cells, respectively. Section is taken at the plane of front servers to show mesh elements as in Fig. 4.

Simulation of server liquid-cooled system

The liquid-cooled system model will be constructed using ANSYS 18.1 [27], CFD analysis. Additionally, simulations will be conducted to assess the impact of copper coating on enhancing the liquid-cooled system. To ensure stability in results and achieve convergence in residuals, transient simulations are performed with time steps of 0.02 s for high-power tanks and 0.1 s for low-power tanks. The multiphase model employs the volume of fluid approach to depict the gas–liquid interface and the motion of vapor bubbles after heat extraction from servers, tracking the volume fraction of each fluid in the domain. A realizable k-ε turbulence model is utilized to characterize turbulence in the system. The liquid FC-72 is employed for two-phase immersion cooling, possessing a low boiling point of 56 °C at atmospheric pressure and a latent heat of vaporization of 88 J.g^{-1}. FC-72 oil is widely used that has high chemical stability, long life-span and high thermal properties. Thermal properties of liquid and vapor phases of FC-72 at its boiling point are detailed in Table 3 [28]. The server walls are constructed from galvanized steel with a thermal conductivity of 51.9 W.m^{-1} °C^{-1}, specific heat of 486 J.kg^{-1} °C^{-1}, and density of 7870 kg.m^{-3}.

Regarding boundary conditions, the heat flux is set for server walls, the top surface of each tank is designated as a pressure outlet, and other tank surfaces are adiabatic. The initial temperature of the liquid oil is set at the boiling point of 56 °C, and the initial volume fraction of the vapor phase is set to zero. The calculated simulation time to reach stability is approximately 20 s for the high-power tank, involving 11,400 iterations, while for the low-power tank; it is around 18 s with 2050 iterations.

To improve the liquid-cooled system, a copper coating is applied to all servers, which has high thermal conductivity (388 W.m^{-1} °C^{-1}). This facilitates efficient heat transfer from the servers to the dielectric liquid, resulting in increased PUE and the maintenance of electronic servers at lower temperatures, thereby extending their service life. The modeling of copper material coating on server walls is executed considering different thicknesses such as 5, 10, 100, 500 μm (μm), and 1 mm for both high and low-power tanks.

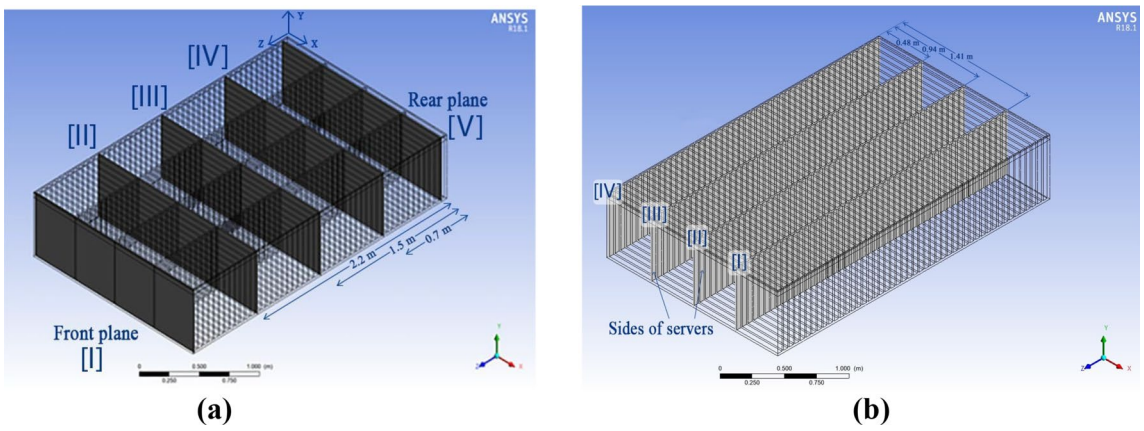


Fig. 7 Planes of **a** *Z*-direction **b** *X*-direction

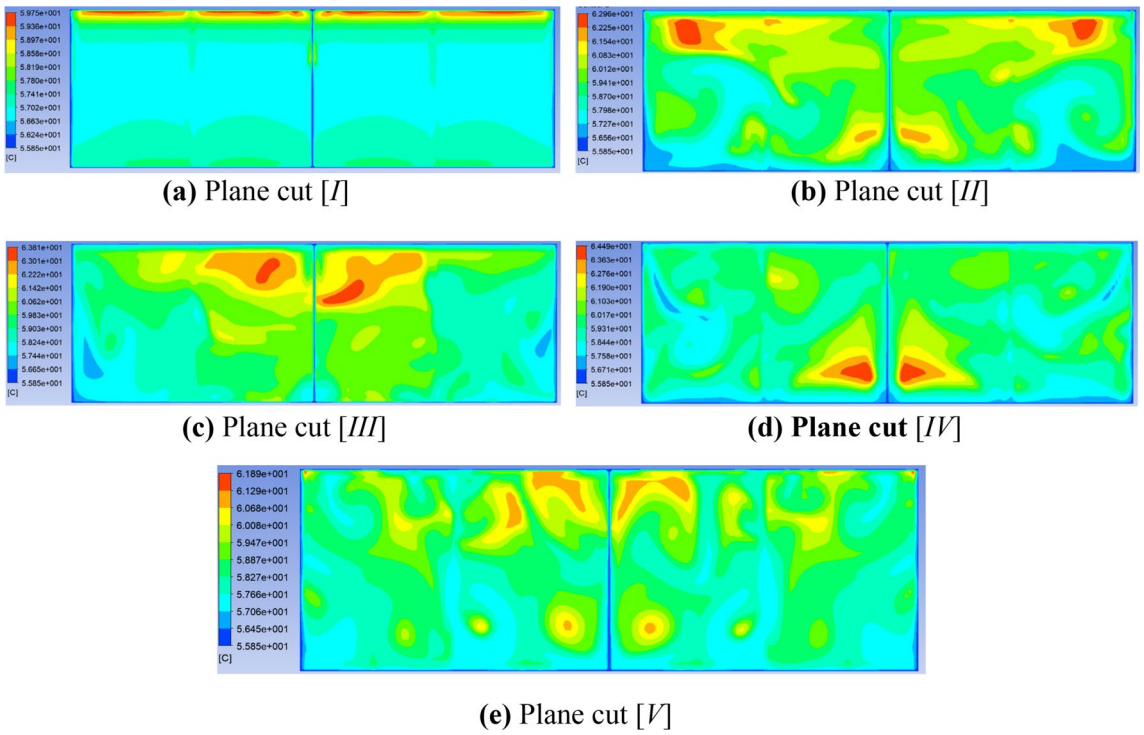


Fig. 8 Temperature distributions of high-power server tank at *Z*-direction

Validation

Priyadumkol and Kittichaikarn [29] simulated the airflow in-row cooling system, especially the inlet rack temperature, to achieve higher efficiency for cooling racks. The layout of the data center, as shown in Fig. 5, is about 25.2 m^2 with a 3.1-m ceiling height. This setup includes two racks, each dissipating 3 kW of heat, along with in-row cooling equipment. The airflow is set to be steady, incompressible, and turbulent, and the three-dimensional model was solved using the standard k–ε turbulence model. The boundary conditions of air from in-row cooling equipment are set as velocity inlet of 1.92 m/s with a temperature of 13 °C. A comparative analysis using Ansys 18.1, CFD was conducted, as depicted in Fig. 6, contrasting the results obtained by Priyadumkol and Kittichaikarn [29] with the outcomes from the proposed simulation. Good agreement has been found with 12% maximum deviation.

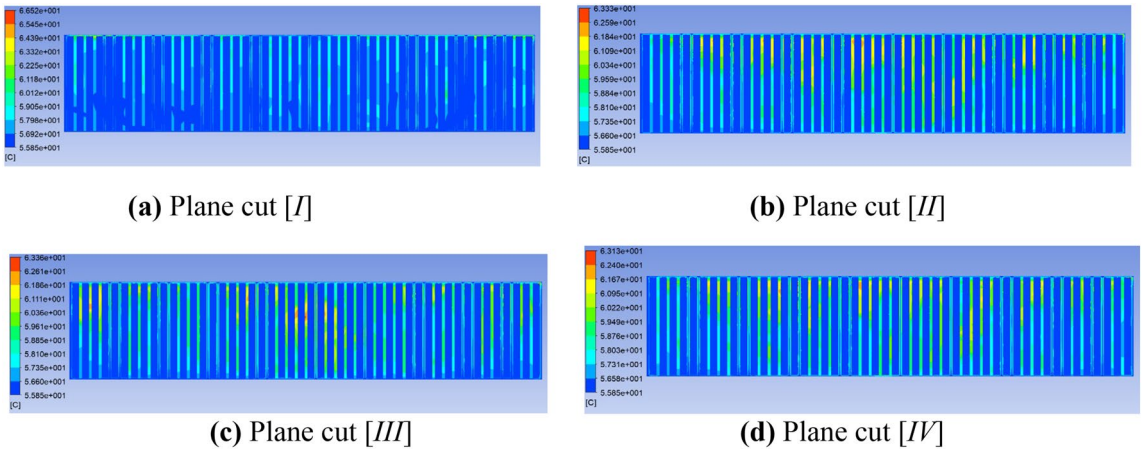


Fig. 9 Temperature distributions of high-power server tank at *X*-direction

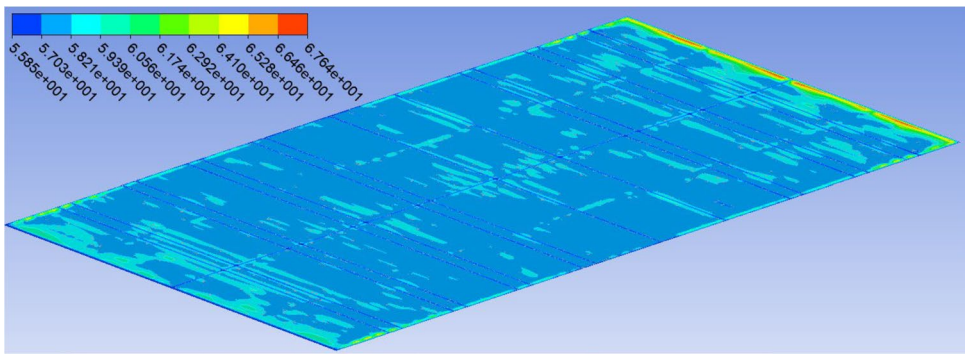


Fig. 10 Temperature distributions of high-power server tank at the server's top

Mathematical model for CFD

The software solves many equations representing the conservation equations and Navier–Stokes equations for a flow to demonstrate the fluid motion and heat transport in three dimensions [30] Mass Conservation (Continuity) equation

$$\frac{\partial \rho}{\partial t} + +div(\rho u) = 0 \tag{1}$$

Momentum equations in *x, y* and *z* directions respectively are

$$\rho \frac{Du}{Dt} = \frac{\partial\left(-p + \tau_{xx}\right)}{\partial x} + \frac{\partial \tau_{yx}}{\partial y} + \frac{\partial \tau_{zx}}{\partial z} + S_{Mx} \tag{2}$$

$$\rho \frac{Dv}{Dt} = \frac{\partial \tau_{xy}}{\partial x} + \frac{\partial\left(-p + \tau_{yy}\right)}{\partial y} + \frac{\partial \tau_{zy}}{\partial z} + S_{My} \tag{3}$$

$$\rho \frac{Dw}{Dt} = \frac{\partial \tau_{xz}}{\partial x} + \frac{\partial \tau_{yz}}{\partial y} + \frac{\partial\left(-p + \tau_{zz}\right)}{\partial z} + S_{Mz} \tag{4}$$

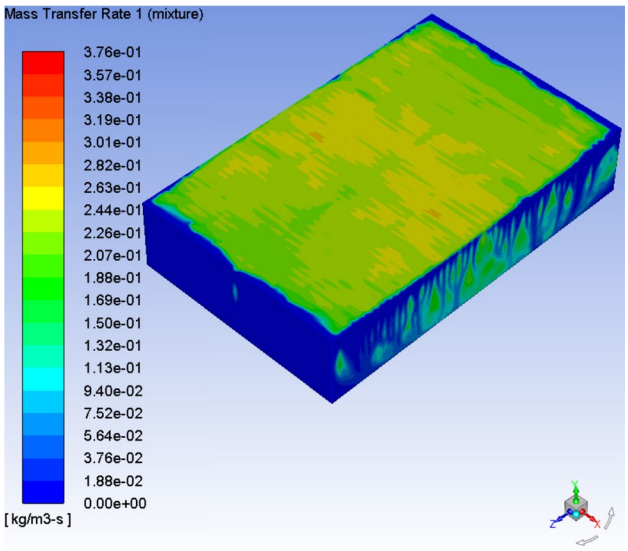


Fig. 11 Mass transfer rate through high-power server tank

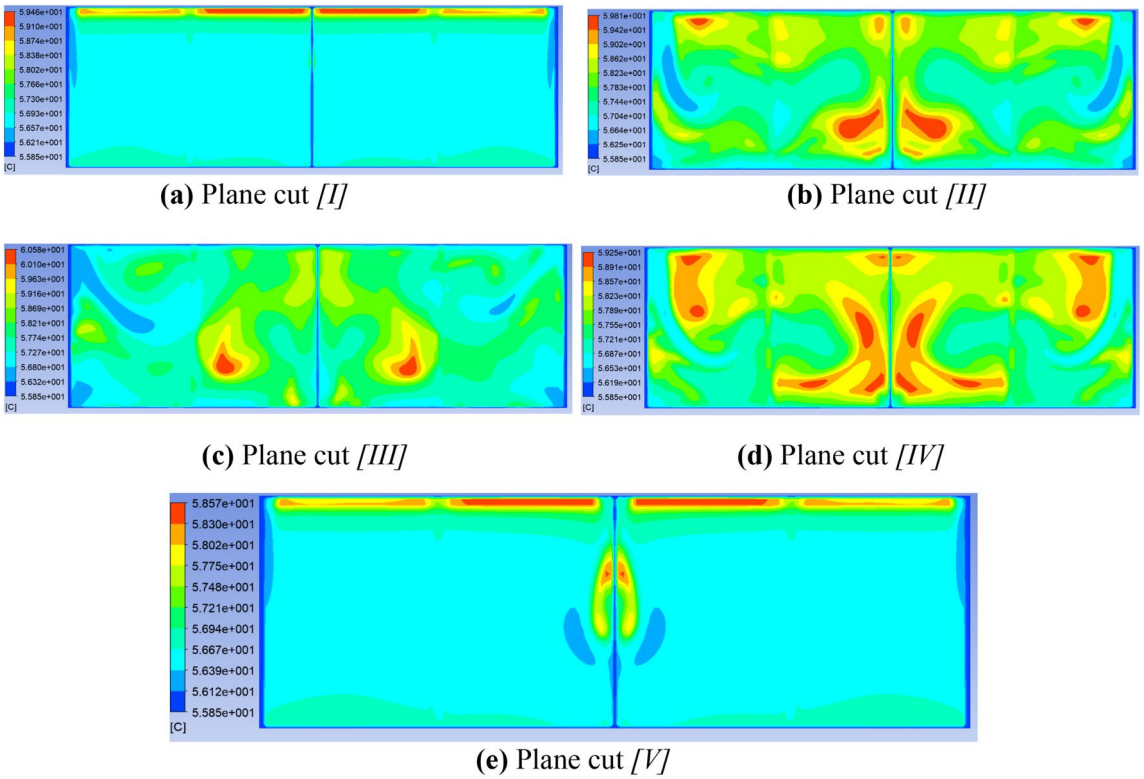


Fig. 12 Temperature distributions of low-power tank at *Z*-direction

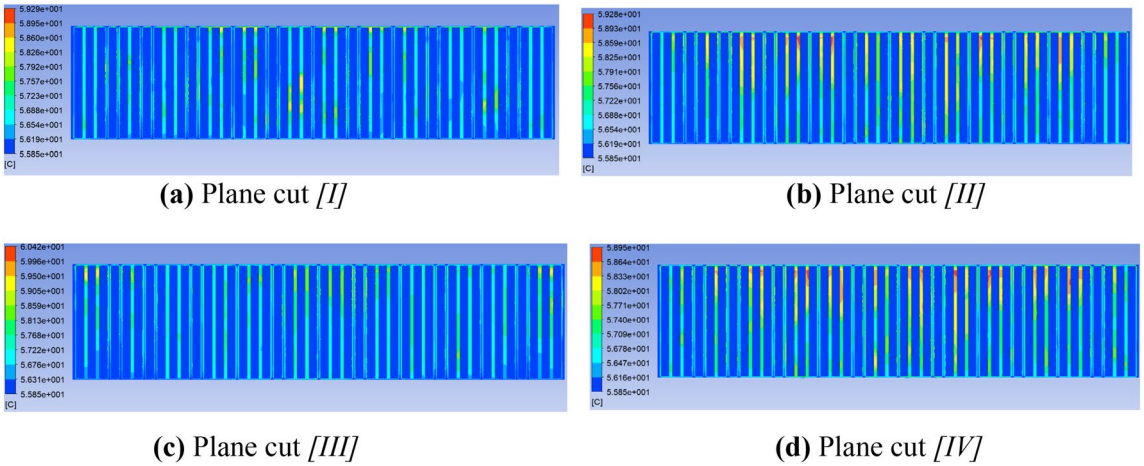


Fig. 13 Temperature distributions of low-power server tank at *X*-direction

Energy equation

$$\rho\frac{DE}{Dt} = -\text{div}(\text{pu}) + \left[\frac{\partial u\tau_{xx}}{\partial x} + \frac{\partial u\tau_{yx}}{\partial y} + \frac{\partial u\tau_{zx}}{\partial z} + \frac{\partial v\tau_{xy}}{\partial x} + \frac{\partial v\tau_{yy}}{\partial y} + \frac{\partial v\tau_{zy}}{\partial z} + \frac{\partial w\tau_{xz}}{\partial x} + \frac{\partial w\tau_{yz}}{\partial y} + \frac{\partial w\tau_{zz}}{\partial z} + \right] + \text{div}\,(k\ \text{grad}\ T) + S_{\text{E}} \quad (5)$$

Turbulence models represent the effect of turbulence in the simulation of fluid flows; the Boussinesq eddy viscosity assumption is considered the basis of all two equations models. *k-ε* turbulence model is considered the most common in the numerical simulations and consists of two transport

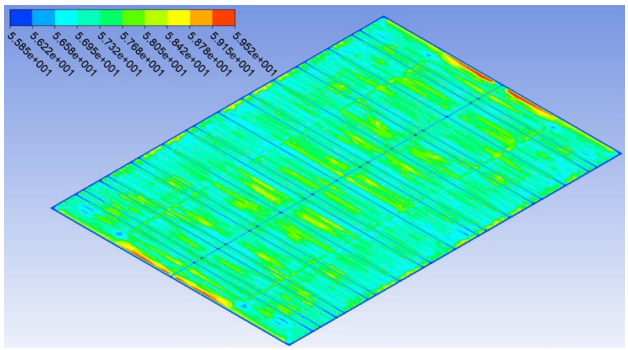


Fig. 14 Temperature distributions of low-power server tank at the server's top

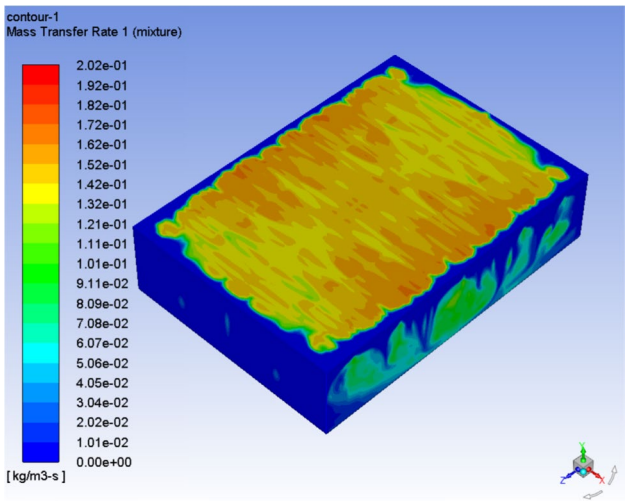


Fig. 15 Mass transfer rate through low-power server tank

parameters, k & ε, that can be calculated from the following equations:

$$\frac{\partial(\rho k)}{\partial t} + \mathrm{div}(\rho k U) = \mathrm{div}\left[\frac{\mu t}{\sigma k}\mathrm{grad}k\right] + 2\mu_{\mathrm{t}}E_{\mathrm{ij}} \cdot E_{\mathrm{ij}} - \rho\varepsilon \quad (6)$$

$$\frac{\partial(\rho\varepsilon)}{\partial t} + \mathrm{div}(\rho\varepsilon U) = \mathrm{div}\left[\frac{\mu t}{\sigma\varepsilon}\mathrm{grad}\varepsilon\right] + C_1\varepsilon\frac{\varepsilon}{K}2\mu_{\mathrm{t}}E_{\mathrm{ij}} \cdot E_{\mathrm{ij}} - C_2\varepsilon\rho\varepsilon^2/k \quad (7)$$

$$\mu_{\mathrm{t}} = \rho C_{\mathrm{M}}k^2/\varepsilon \quad (8)$$

where C_{M}, C_1 ε and C_2 ε are constants.

Volume of the fluid model is used to simulate the boiling process in the tank. Both vapor and liquid phases are assumed to behave as continuous media in this multiphase flow model. Eulerian–Eulerian approach is applied, Hertz–Knudsen stated equation [31] for the net mass flux over the vapor–liquid interphase during the evaporation process.

$$J = \alpha_{\mathrm{c}}\frac{\sqrt{M}}{\sqrt{2\Pi R}}\left(\frac{p}{\sqrt{T_{\mathrm{v}}}} - \frac{p_{\mathrm{sat}}\,T_{\mathrm{l}}}{\sqrt{T_{\mathrm{l}}}}\right) \quad (9)$$

Results and discussion

Simulation results state temperature distribution contours for electronic servers at various planes and quantify the vapor produced during the cooling process. Additionally, the power usage of the systems is clarified. A comparative analysis between liquid and air-cooled systems is conducted, and the impact of coating on the cooling performance of both high and low-power servers is explored. The optimal coating thickness is selected to achieve the most effective enhancement.

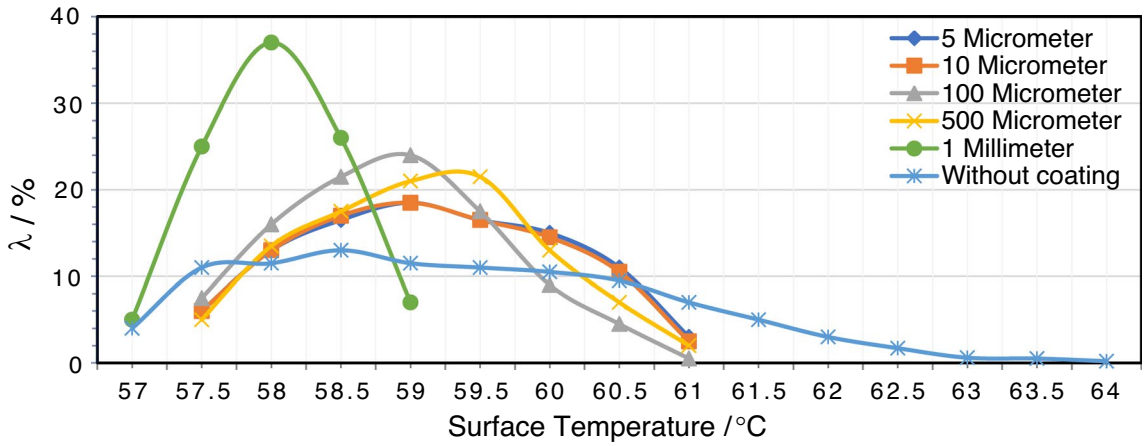


Fig. 16 Effect of coating thickness on temperature distribution for high-power tank

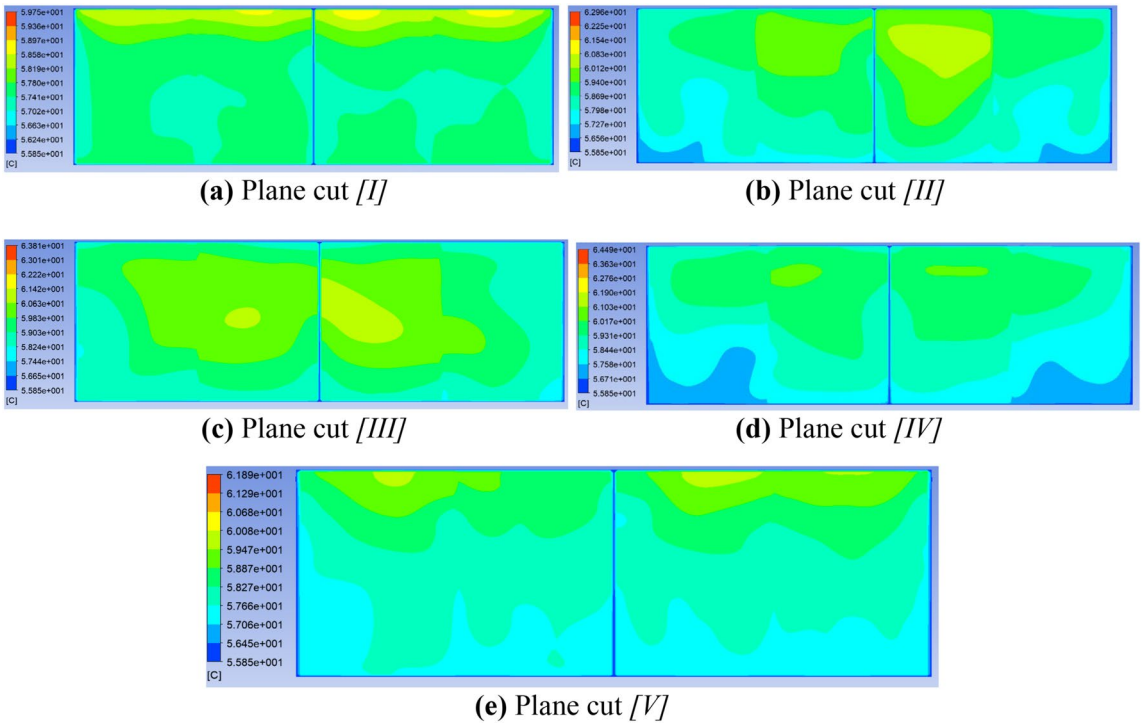


Fig. 17 Temperature distribution of coated high-power server tank, *Z*-direction

Liquid-cooled simulation

For high-power servers, five planes are taken in *Z*-direction at different distances and four planes in *X*-direction, as shown in Fig. 7.

The temperature distribution of the high-power server tank is illustrated at various locations in the *X*–*Y* plane as depicted in Fig. 8. In the *Z*-direction, heat transfer is nonuniform, leading to the formation of hot spots due to boiling. Small bubbles near the server walls are initiated, and a majority of these bubbles grow. At servers positioned in front of the tank [*I*], the lowest temperature distribution is observed, approximately around 57 °C. However, hot spots exceeding 59.7 °C are present at the top of four servers, attributed to the accumulation of vapor bubbles on the top surface. Moving to the second plane [*II*], temperatures increase to 63 °C at specific hot spots located on the top sides and near the middle of servers at 61.5 °C. The highest temperature distribution occurs at the middle plane of tank [*III*] and at plane [*IV*], surpassing 64 °C in the vicinity of the middle area of servers. At the rear servers, the temperature decreases to less than 58 °C, yet numerous random

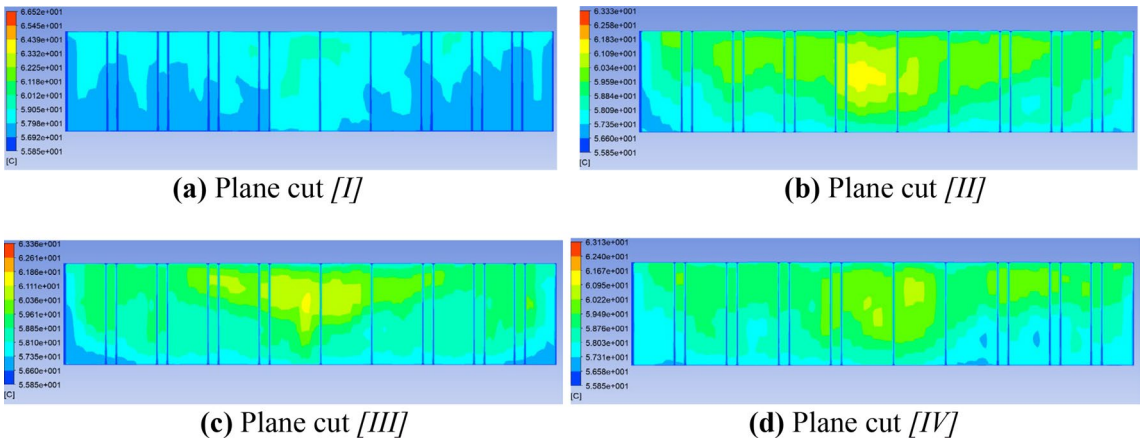


Fig. 18 Temperature distribution of coated high-power server tank, *X*-direction

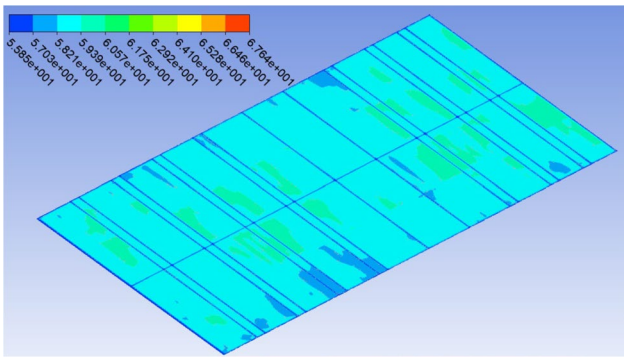


Fig. 19 Temperature distributions of coated high- power server tank at the server's top

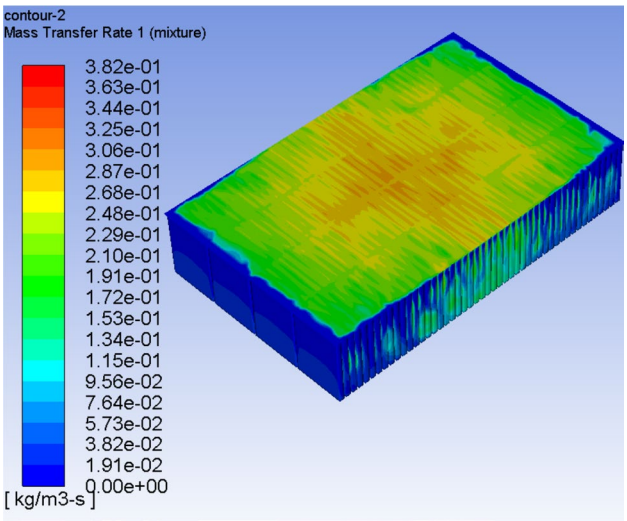


Fig. 20 Mass transfer rate through coated high-power server tank

hot spots at 61 °C. Regarding the X-direction, as illustrated in Fig. 9, the sides of servers exhibit lower temperatures, approximately around 57 °C, while the temperature of the oil vapor phase between servers increases.

Figure 10 illustrates the temperature distribution in *Y*-direction at the top surface of servers, with an average temperature exceeding 57 °C, except for a specific spot on one side that reaches above 67 °C. The vapor phase accumulates at the top surface of servers, exhibiting an average mass flow rate of 0.25 kg m^{-3}, as depicted in Fig. 11. This vapor phase will condense in the heat exchanger cycle, contributing to a power of 860 Watts for each high-power tank.

For Low-power servers, Sections in the *X*-direction are analyzed similarly to high-power tanks, and five planes are intersected in the *Z*-direction at different distances, encompassing front servers, 1.98 m, 1.3 m, 0.6 m and at rear servers.

In the *Z*-direction, as shown in Fig. 12, the front and rear servers exhibit lower temperatures, while hot spots are concentrated at the top of servers, exceeding 59 °C. Conversely, three other planes at different distances have higher temperatures, with random hot spots dispersed across the surfaces of servers, particularly at the top and middle, surpassing 60 °C. From Fig. 13, the sides of servers shown in the *X*-direction are at temperature of 56 °C. However, the vapor bubbles between them show an increase from the boiling point to 60 °C. Figure 14 explains that the temperature distribution of top surfaces is about 57 °C for most areas. The average mass flow rate of vapor phase is approximately 0.17 kg m^{-3}. S as in Fig. 15, at a temperature of 57 °C, with a power requirement of 500 Watts for each low-power tank.

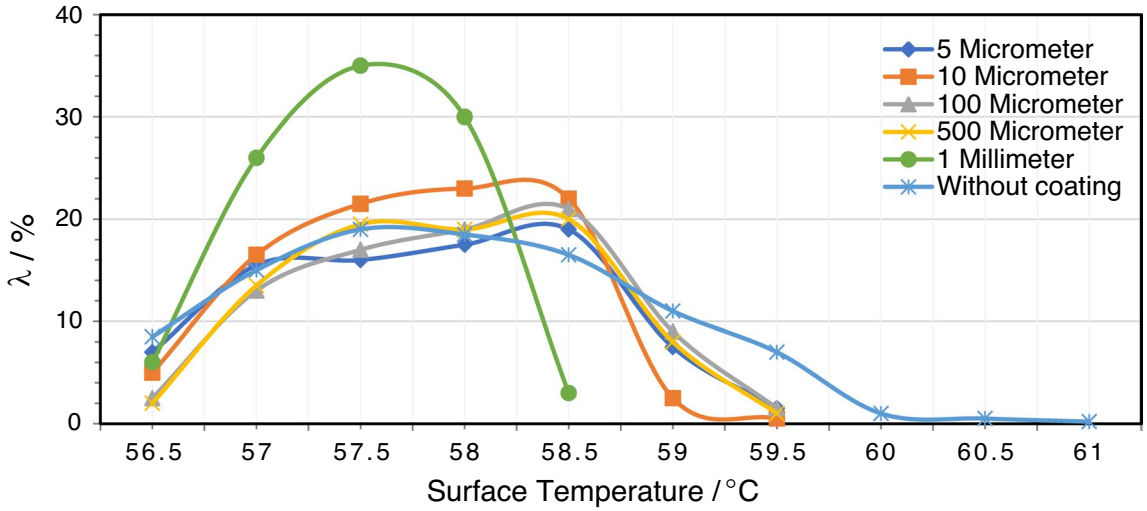


Fig. 21 Effect of coating thickness on temperature distribution for low-power tank

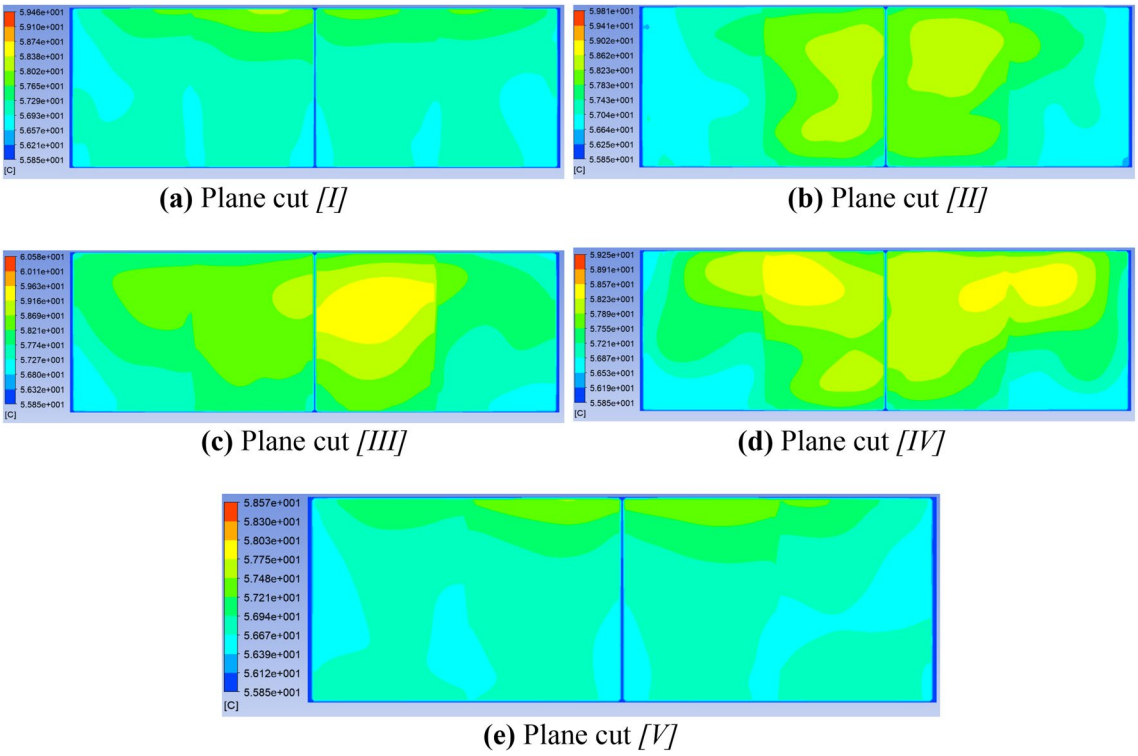


Fig. 22 Temperature distribution of coated low-power server tank, *Z*-direction

Coating thickness effect on cooling performance

For high-power servers, the impact of coating all servers with thicknesses 5,10,100,500 µm and 1 mm on temperature distribution percentage is illustrated in Fig. 16. Additionally, a comparison between the coating effects and a system without coating is presented. Temperature distribution percentage (λ) signifies the area occupied by contours representing various surface temperatures. All different coating thicknesses result in the reduction of higher temperatures in hot spots, limiting the maximum temperatures to 61 °C, except for the 1 mm thickness, which restricts it to 59 °C. Among the various thicknesses, the 100 µm coating exhibits an optimized heat transfer effect, yielding a higher percentage increase in lower temperatures without the need for a thicker copper layer, such as the 1 mm option. The 100 µm thickness indicates a maximum improvement of approximately 13% compared to servers without coating and represents the lowest temperature distribution percentage for temperatures exceeding 60 °C. Coating high-power servers with copper particles at a size of 100 µm results in a 1 °C decrease at the

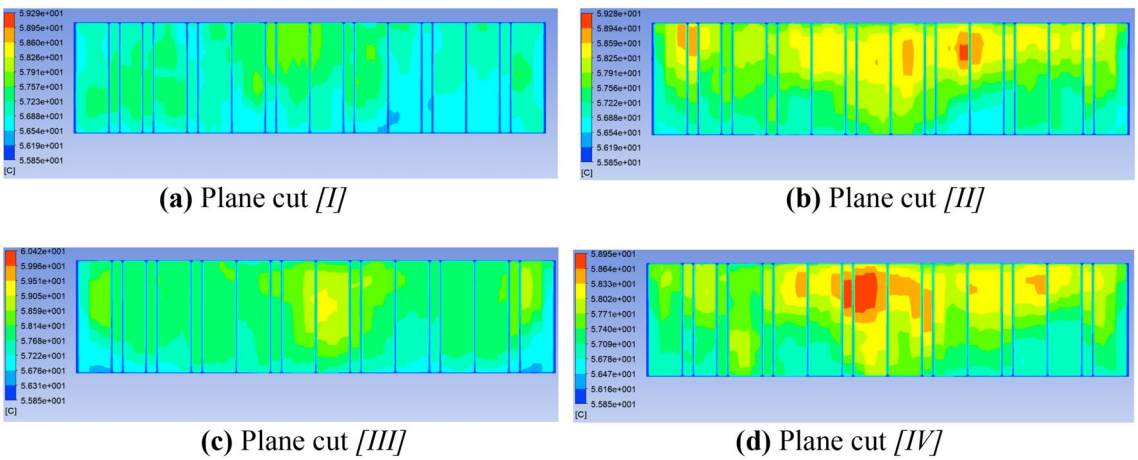


Fig. 23 Temperature distribution of coated high-power server tank, *X*-direction

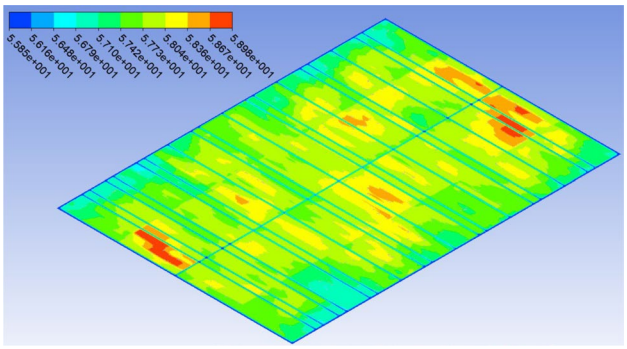


Fig. 24 Temperature distributions of coated low- power server tank at the server's top

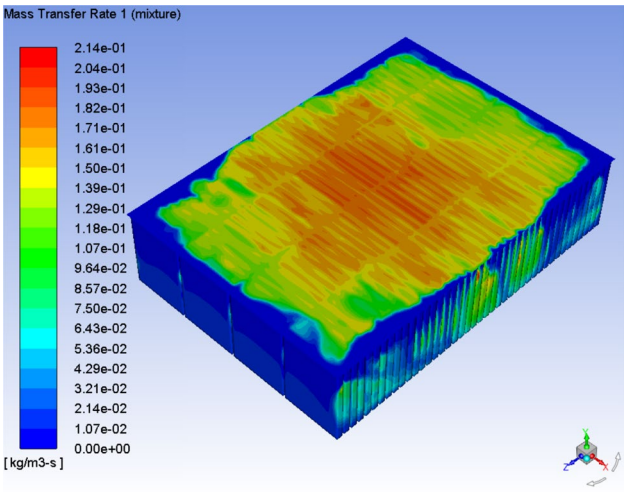


Fig. 25 Mass transfer rate through coated low-power server tank

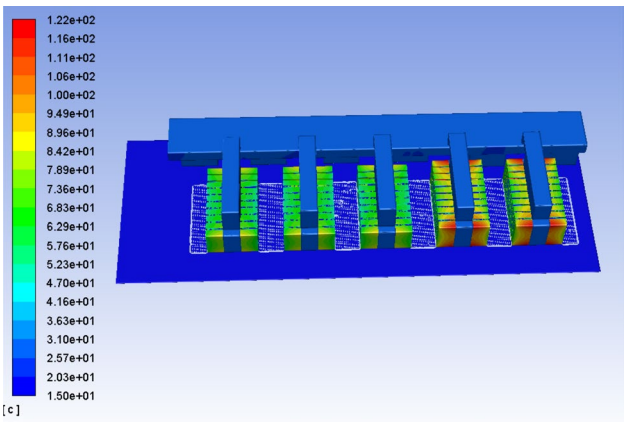


Fig. 26 Temperature distribution of air-cooled racks

top hot spots for the front servers [*I*], as displayed in Fig. 17 in the *Z*-direction. For plane [*II*], coating eliminates all hot spots except for one region with a maximum temperature of 60 °C, and the temperature distribution is more uniform than servers without coating. For plane [*III*], the temperature of 100 µm coating servers gradually increases near the middle of servers with elimination of hot spots except for a small area of 61 °C, indicating enhancement. For the last two planes, coating eliminates the hot spots and decreases temperature. However, planes in the *X*-direction show that temperature increases by 1–3 °C compared to that without coating, as shown in Fig. 18. At top surface of servers, as shown in Fig. 19, temperature increases about 1 °C compared to the state before coating. The flow rate of vapor phase in Fig. 20 exhibits similarity to the system before coating, indicating the same power requirement for the high-power tank before adding the copper coating.

In the case of low-power servers, the maximum temperatures of hot spots decrease by 1.5 °C for various coating thicknesses, as described in Fig. 21, and by 2.5 °C for 1 mm thickness. The thickness of 10 µm demonstrates a higher improvement percentage, approximately 8%. Additionally, it exhibits the lowest temperature distribution above 58.5 °C until it reaches the.

Maximum point above 59 °C, covering a minimal area within the contours.

Temperature distribution contours of 10 µm coating are shown in Figs. 22 and 23. In the *Z*-direction, plane [*I*] exhibits lower temperatures with a small area of maximum hot spots at 58 °C, similar to the rear servers; the maximum temperature at the top is approximately 57.5 °C. Planes [*II*] and [*III*] have higher temperatures that increase from the outer sides to the middle with a uniform distribution and maximum hot spots reaching 59 °C. The plane at [*IV*] has a larger area with a maximum temperature of 58.5 °C. For *X*-direction, the coated server sides have higher temperatures compared to before coating. Figure 24 explains some hot spots above 58 °C at the servers' top.

At the top surfaces of high and low-power tanks, the mass transfer rate of vapor phase remains consistent with the system without coating, as in Fig. 25. The total power required for all tanks after coating is about 16 kW, indicating that PUE remains nearly unchanged, standing at around 1.01. Consequently, the coating on servers enhances heat transfer without introducing additional operating costs to the system.

Air-cooled simulation

The simulation is performed for the optimal case in the study utilizing a cooling system with a raised floor and HAC. In the hot aisles, the air temperature difference ranges from 26 to 30 °C. Within the six rows of low-power racks, the temperature gradually increases from 55 °C at the rack walls adjacent to cold aisles to 80 °C closer to hot aisles. The hot spots reach about 90 °C at the sides of the front and rear

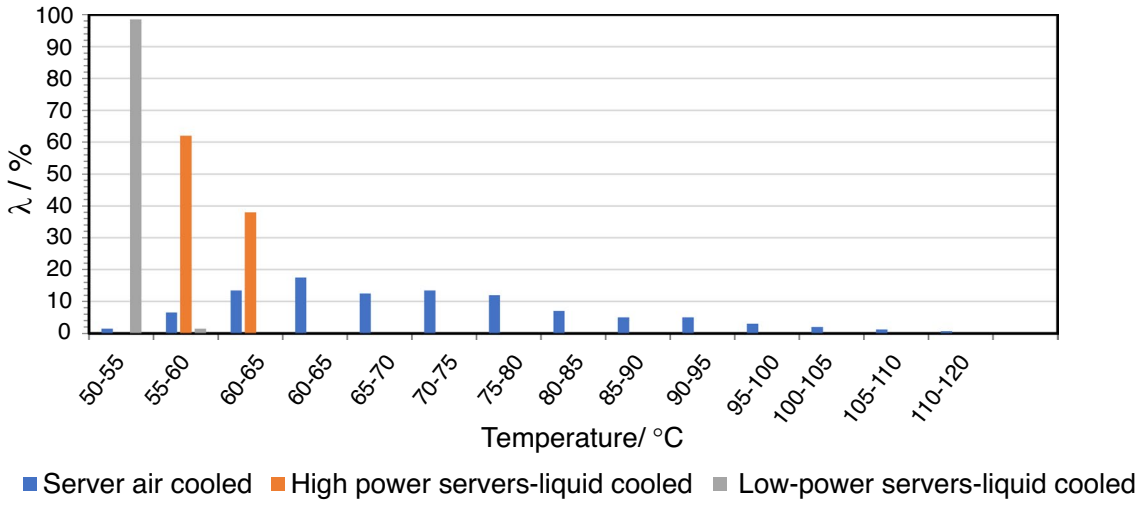


Fig. 27 Effect of cooling types on temperature

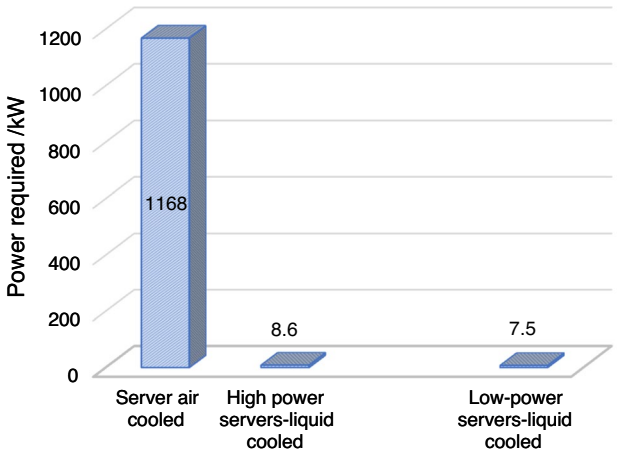


Fig. 28 Power consumption for different cooling systems

racks near hot aisles. In the air system, these hot spots arise due to the nonuniform distribution of airflow across various walls of the racks. For the four rows of high-power racks, the temperature range rises gradually from 65 °C to 122 °C, with the majority falling between 75 °C and 90 °C, as in Fig. 26. The operational net cooling power of air conditioners is 1168 kW, as mentioned in the paper [26], resulting in PUE of approximately 2 for HAC system with a raised floor during normal operation.

Comparison between air-cooled and liquid-cooled systems

Simulation results show a significant effect of cooling with liquid oil compared to air cooling. Illustrated in Fig. 27 is the difference in temperature ranges between liquid cooling and air cooling. It is evident that liquid cooling restricts temperatures to 65 °C, whereas air cooling results in approximately 60% of rack surfaces ranging from 65 °C to 120 °C. Server liquid cooling not only improves power efficiency but also reduces PUE from 2 in the case of air cooling to 1.01, thereby lowering electricity running costs. As described in Fig. 28, liquid cooling achieves a remarkable 99% reduction in power consumption for cooling when compared to air conditioners. In terms of modeling, the liquid-cooled system occupies a space approximately 50% smaller than the air-cooled system.

Conclusions

Numerical simulation utilizing ANSYS18.1, CFD, was employed to compare the cooling effectiveness of liquid cooling and air cooling, yielding the following findings:

- The simulation of air cooling, employing the optimal configuration with a raised floor and hot aisle containments. Temperatures for low-power racks range from 50 °C to 90 °C, while higher power racks exhibit temperature ranges between 65 °C and 122 °C. Hot spots are more prominent due to nonuniform distribution of air flow.
- The simulation of two-phase immersion liquid cooling with FC-72 dielectric oil demonstrates a significant improvement for low-power server tanks, with temperatures ranging from 56 °C to maximum hot spots below 61 °C. For higher power servers, temperature ranges are between 56 °C and 65 °C at maximum hot spots. The heat transfer enhancement is attributed to the higher heat transfer coefficient of the oil compared to air.

- The total power consumption for all high-power tanks is approximately 8.5 kW, while for low-power tanks, it is 7.5 kW. Consequently, the PUE of liquid cooling is about 1.01, representing a 50% reduction compared to air cooling with a PUE of 2. This enhancement leads to electricity savings and lower operational costs.
- The liquid-cooled system reduces design and control complexities, occupies less space, and contributes to environmental preservation by minimizing CO_2 emissions due to reduced power consumption.
- Copper coating of servers enhances temperature distribution uniformity and eliminates hot spots owing to its higher thermal conductivity. The coating is particularly advantageous for high-power servers, decreasing the maximum temperature by 3 °C, and for low-power servers, reducing it by 1.5 °C. The maximum improvement percentages for high-power and low-power servers are 13% and 8%, respectively.
- The PUE of servers with copper coating is approximately 1.01, comparable to the power of servers without coating.

For future work, the research should focus on studying the complete cycle of the liquid cooling system, including heat exchangers, pumps, and pipes, to analyze the system's efficiency. Studying how the use of different new technologies of dielectric oils affects cooling performance.

Authors contribution Nada M. Mohammed done software, writing—original draft, visualization, data curation, resources. Mohamed Elhelw* contributed to conceptualization, investigation; methodology; supervision, writing. Wael El-maghlany helped in project administration, supervision, writing—review & editing. Ahmed H. Abdelaziz was involved in investigation, supervision, writing, methodology, original draft original draft.

Funding Open access funding provided by The Science, Technology & Innovation Funding Authority (STDF) in cooperation with The Egyptian Knowledge Bank (EKB).

Open Access This article is licensed under a Creative Commons Attribution 4.0 International License, which permits use, sharing, adaptation, distribution and reproduction in any medium or format, as long as you give appropriate credit to the original author(s) and the source, provide a link to the Creative Commons licence, and indicate if changes were made. The images or other third party material in this article are included in the article's Creative Commons licence, unless indicated otherwise in a credit line to the material. If material is not included in the article's Creative Commons licence and your intended use is not permitted by statutory regulation or exceeds the permitted use, you will need to obtain permission directly from the copyright holder. To view a copy of this licence, visit http://creativecommons.org/licenses/by/4.0/.

References

1. Mukaffi ARI, Arief RS, Hendradjit W, Romadhon R. Optimization of cooling system for data center case study: PAU ITB data center. Procedia Eng. 2017;170:552–7. https://doi.org/10.1016/j.proeng.2017.03.088.
2. Kang D, Lee J, Chakraborty A, Lee S, Kim G, Yu C. Recent advances in two- phase immersion cooling with surface modifications for thermal management. Energies. 2022;15(3):1214. https://doi.org/10.3390/en15031214.
3. Ni J, Bai X. A review of air conditioning energy performance in data centers. Renew Sustain Energy Rev. 2017;67:625–40. https://doi.org/10.1016/j.rser.2016.09.050.
4. Marcinichen JB, Olivier JA, Thome JR. On-chip two-phase cooling of datacenters: cooling system and energy recovery evaluation. Appl Therm Eng. 2012;41:36–51. https://doi.org/10.1016/j.applthermaleng.2011.12.008.
5. Capozzoli A, Primiceri G. Cooling systems in data centers: state of art and emerging technologies. Energy Procedia. 2015;83(2):484–93. https://doi.org/10.1016/j.egypro.2015.12.168.
6. Bhopte S, Sammakia B, Schmidt R, Iyengar M K, Agonafer D. Effect of under floor blockages on data center performance. 2006; 426–433. https://doi.org/10.1109/ITHERM.2006.1645374.
7. Fulpagare Y, Bhargav A, Joshi Y. Dynamic thermal characterization of raised floor plenum data centers: experiments and CFD. J Build Eng. 2019;25: 100783. https://doi.org/10.1016/j.jobe.2019.100783.
8. ASHRAE Technical Committee. Thermal Guidelines for Data Processing Environments-Expanded Data Center Classes and Usage Guidance. ASHRAE, Tech. Rep. 2011; 679.
9. Lee KP, Chen HL. Analysis of energy saving potential of air-side free cooling for data centers in worldwide climate zones. Energy Build. 2013;64:103–12. https://doi.org/10.1016/j.enbuild.2013.04.013.
10. Zhang C, Sun X, Han Z, Li X, Dong J. Energy saving potential analysis of two-phase immersion cooling system with multi-mode condenser. Appl Therm Eng. 2023;219: 119614. https://doi.org/10.1016/j.applthermaleng.2022.119614.
11. Cheong KH, Tang KJW, Koh JM, Yu SCM, Acharya UR, Xie NG. A Novel methodology to improve cooling efficiency at data centers. IEEE. 2019. https://doi.org/10.1109/ACCESS.2019.2946342.
12. Ni J, Jin B, Zhang B, Wang X. Simulation of thermal distribution and airflow for efficient energy consumption in a small data centers. Sustainability. 2017;9(4):664. https://doi.org/10.3390/su9040664.
13. Herrlin MK. Rack cooling effectiveness in data centers and telecom centraloffices: the rack cooling index (RCI). ASHRAE Transactions 111 (Part 2). American Society of Heating, Refrigerating and Air-Conditioning Engineers,Inc. Atlanta, GA; 2005.
14. Moazamigoodarzi H, Gupta R, Pal S, Tsai PJ, Ghosh S, Puri IK. Modeling temperature distribution and power consumption in IT server enclosures with row-based cooling architectures. Appl Energy. 2020;261: 114355. https://doi.org/10.1016/j.apenergy.2019.114355.
15. Jin C, Bai X, An Y, Ni J, Shen J. Case study regarding the thermal environment and energy efficiency of raised-floor and row-based cooling. Build Environ. 2020;182(5): 107110. https://doi.org/10.1016/j.buildenv.2020.107110.
16. Pambudi NA, Sarifudin A, Firdaus RA, Ulfa DK, Gandidi IM, Romadhon R. The immersion cooling technology: current and future development in energy saving. Alex Eng J. 2022;61(12):9509–27. https://doi.org/10.1016/j.aej.2022.02.059.
17. Dumitrescu C, Plesca A, Dumitrescu L, Adam M, Nituca C, Dragomir A. Assessment of data center energy efficiency. Methods

Metrics IEEE. 2018. https://doi.org/10.1109/ICEPE.2018.8559745.
18. Zhang Y, Li C, Pan M. Design and performance research of integrated indirect liquid cooling system for rack server. Int J Therm Sci. 2022;184(4): 107951. https://doi.org/10.1016/j.ijthermalsci.2022.107951.
19. Kuncoro IW, Pambudi N, Biddinika MK, Widiastuti I, Hijriawan M, Wibowo KM. Immersion cooling as the next technology for data center cooling: a review. J Phys: Conf Ser. 2019;1402(4): 044057. https://doi.org/10.1088/1742-6596/1402/4/044057.
20. Liu C, Yu H. Evaluation and optimization of a two-phase liquid-immersion cooling system for data centers. Energies. 2021;14(5):1395. https://doi.org/10.3390/en14051395.
21. An X, Arora M, Huang W, Brantley WC, Greathouse JL. 3D numerical analysis of two-phase immersion cooling for electronic components. IEEE. 2018. https://doi.org/10.1109/ITHERM.2018.8419528.
22. Watson B, Venkiteswaran VK. Universal cooling of data centres: A CFD analysis. Energy Procedia. 2017;142:2711–20. https://doi.org/10.1016/j.egypro.2017.12.215.
23. Eiland R, Fernandes JE, Vallejo M, Siddarth A, Agonafer D, Mulay V. Thermal performance and efficiency of a mineral oil immersed server over varied environmental operating conditions. J Electron Packaging. 2017. https://doi.org/10.1115/1.4037526.
24. Luo Q, Wang C, Wu C. Study on heat transfer performance of immersion system based on SiC/white mineral oil composite nanofluids. Int J Therm Sci. 2023;187: 108203. https://doi.org/10.1016/j.ijthermalsci.2023.108203.
25. Ali A. Thermal Performance and stress analysis of heat spreaders for immersion cooling applications. Appl Therm Eng. 2020;181(21):115984. https://doi.org/10.1016/j.applthermaleng.2020.115984.
26. Cho J, Woo J, Park B, Lim T. A comparative CFD study of two air Distribution systems with hot aisle containment in high-density data centers. Energies. 2020;13(22):6147. https://doi.org/10.3390/en13226147.
27. ANSYS, Inc. ANSYS Fluent Tutorial Guide, Release 18; 2017.
28. Niazmand A, Chauhan T, Saini S, Shahi P, Bansode P V, Agonafer D. CFD Simulation of Two-Phase Immersion Cooling Using FC-72 Dielectric Fluid. Conference: ASME 2020 International Technical Conference and Exhibition on Packaging and Integration of Electronic and Photonic Microsystems; 2020. https://doi.org/10.1115/IPACK2020-2595.
29. Priyadumkol J, Kittichaikarn C. Application of the combined air-conditioning systems for energy conservation in data center. Energy Build. 2014;68:580–6. https://doi.org/10.1016/j.enbuild.2013.07.082.
30. Versteeg HK, Malalasekera W. An Introduction to Computational Fluid Dynamics, The Finite Volume Method. Second Edition; 2007.
31. De Schepper SCK, Heynderickx GJ, Marin GB. Modeling the evaporation of a hydrocarbon feedstock in the convection section of a steam cracker. Comput Chem Eng. 2009;33(1):122–32. https://doi.org/10.1016/j.compchemeng.2008.07.013.

Publisher's Note Springer Nature remains neutral with regard to jurisdictional claims in published maps and institutional affiliations.